# Assessment of Frequency-Dependent Alterations in the Level of Extracellular $Ca^{2+}$ in the Synaptic Cleft

Peter M. Vassilev, Jude Mitchel, Michael Vassilev, Marie Kanazirska, and Edward M. Brown
Endocrine-Hypertension Division, Department of Medicine, Brigham and Women's Hospital and Harvard Medical School, Boston, Massachsetts 02115 USA

ABSTRACT The synaptic cleft may be represented as a very thin disk of extracellular fluid. It is possible that at high stimulation frequencies the interval between pulses would be insufficient for diffusion of $Ca^{2+}$ from the periphery of the cleft to replace extracellular $Ca^{2+}$ depleted at the center of the cleft as a result of activation of postsynaptic, $Ca^{2+}$-permeable channels. Computer modeling was employed to assess the impact of activation of glutamate receptor channels (GRCs) in the postsynaptic membrane on the level of extracellular $Ca^{2+}$ within the synaptic cleft. The model includes calcium influx from the synaptic cleft into the postsynaptic compartment through GRC and calcium efflux through calcium pumps and Na/Ca exchangers. Concentrations of extracellular $Ca^{2+}$ inside the cleft are estimated by using a compartmental model incorporating flux across the postsynaptic membrane and radial diffusion from the edges of the cleft. The simulations suggest that substantial extracellular $Ca^{2+}$ depletion can occur in the clefts during activation of GRCs, particularly at high stimulation frequencies used to induce long-term potentiation (LTP). Only minimal transitory changes in extracellular $Ca^{2+}$ are observed at low frequencies. These frequency-dependent alterations in extracellular $Ca^{2+}$ dynamics are a direct reflection of the activity of GRCs and could be involved in the modulation of presynaptic function via a retrograde messenger mechanism, if there are extracellular $Ca^{2+}$ sensors on the presynaptic membranes. The recently cloned extracellular $Ca^{2+}$-sensing receptors that are known to be present in nerve terminals in hippocampus and other areas of the brain could potentially play such a role.

## INTRODUCTION

It is well established that the entry of $Ca^{2+}$ through *N*-methyl-D-aspartate (NMDA) channels and other ionotropic glutamate receptor (iGluR) channels plays a crucial role in the mechanism underlying synaptic enhancement in the hippocampus, particularly at synapses between the presynaptic terminals of the Schafer collaterals of CA3 neurons and the postsynaptic, dendritic spines of CA1 pyramidal neurons (Bliss and Collingridge, 1993). An elevation in the cytosolic $Ca^{2+}$ concentration in these spines as a result of $Ca^{2+}$ influx through NMDA channels is thought to be a major factor in the induction of long-term potentiation (LTP) in this region of hippocampus (Malenka et al., 1988; Bekkers and Stevens, 1989; Malgaroli and Tsien, 1992; Jahr and Stevens, 1993). $Ca^{2+}$ influx within or in close proximity to synaptic clefts likewise plays an important role in all steps of synaptic transmission, at both presynaptic and at postsynaptic levels (Bliss and Collingridge, 1993; Bolshakov and Siegelbaum, 1994). Available evidence supports the existence of one or more transsynaptic, retrograde messengers that modulate presynaptic glutamate release (Malinow and Tsien, 1990; Bekkers and Stevens, 1990; Bliss and Collingridge, 1993). This putative retrograde signaling system acts to coordinate postsynaptic changes in cytosolic $Ca^{2+}$ with presynaptic release of neuromediators, such that increases in postsynaptic cytosolic $Ca^{2+}$ further stimulate glutamate release. Such an amplification mechanism may underlie synaptic enhancement during the induction of LTP by high-frequency (100 Hz) electrical stimulation. Moreover, recent studies of homosynaptic systems, in which LTP was generated by high-frequency pulses, have shown that the opposite type of synaptic plasticity, long-term depression (LTD), could be induced by decreasing the frequency of stimulation to 1–5 Hz (Dudek and Baer, 1992).

Previous models have explored frequency-dependent changes in cytosolic $Ca^{2+}$ in postsynaptic spines as a result of influx via NMDA and other channels as possible mediators of LTP and LTD (Gamble and Koch, 1987; Holmes, 1990; Holmes and Levy, 1990; Zador et al., 1990). These have included detailed analyses of the dynamic alterations in cytosolic $Ca^{2+}$ within various postsynaptic compartments (e.g, the head and neck of dendritic spines) (Kitajima and Hara, 1990; Koch and Zador, 1993; Zador and Koch, 1994; Schiegg et al., 1995). To date, however, the role of associated changes in extracellular $Ca^{2+}$, especially within the synaptic cleft, have not been examined, despite abundant evidence that extracellular $Ca^{2+}$ within the narrow intercellular spaces of the brain can change dramatically with neuronal excitation and changes in synaptic activity (Hamon and Heinemann, 1986; Arens et al., 1992; Lucke et al., 1995). It was shown, for example, that activation of NMDA channels can mediate depletion of extracellular $Ca^{2+}$ from normal levels to less than 1.0 mM in hippocampal slices (Arens et al., 1992). Activity-dependent extracellular $Ca^{2+}$ depletion has also been described with other

*Received for publication 3 September 1996 and in final form 28 January 1997.*

Address reprint requests to Dr. Peter M. Vassilev, Endocrine-Hypertension Division, Brigham and Women's Hospital and Harvard Medical School, 221 Longwood Ave., Boston, MA 02115. Tel.: 617-732-5587; Fax: 617-732-5764.



0006-3495/97/05/2103/14 $2.00

excitable cells (Almers et al., 1981; Bers, 1983; Cleeman et al., 1984; Dresdner and Kline, 1985; Hilgemann, 1986).

We recently cloned a phosphatidyl inositol (PI)- and G protein-coupled, $Ca^{2+}$-sensing receptor (CaR) from parathyroid (Brown et al., 1993) and kidney (Riccardi et al., 1995), which is present in various regions of the brain (including synaptic regions of the hippocampus) and could potentially sense fluctuations in extracellular $Ca^{2+}$ within the brain (Ruat et al., 1995; Brown et al., 1995). The CaR bears substantial homology to the metabotropic glutamate receptors (mGluRs) (Brown et al., 1993; Riccardi et al., 1995; Ruat et al., 1995). In the parathyroid, the CaR senses minute changes (2–3%) in extracellular $Ca^{2+}$ by virtue of the steep inverse sigmoidal relationship between extracellular $Ca^{2+}$ and receptor activation in the physiological range (e.g., 1.0–1.5 mM extracellular $Ca^{2+}$) (Brown, 1991; Brown et al., 1993). Thus the activity-dependent changes in extracellular $Ca^{2+}$ within the brain are more than sufficient to modulate the activity of CaRs in the vicinity of excited synaptic membranes (Brown et al., 1995).

In the present study we used computer modeling to explore the possibility that similar changes in extracellular $Ca^{2+}$ could also take place within the synaptic cleft during activation of iGluRs and other $Ca^{2+}$-permeable channels. Because of the lack of suitable methods for measuring extracellular $Ca^{2+}$ in synaptic clefts, modeling is a useful approach to examining the possible role of various factors in modulating extracellular $Ca^{2+}$ in these functionally important intercellular spaces. Our simulations suggest that substantial extracellular $Ca^{2+}$ depletion may occur in the clefts during activation of NMDA channels, particularly at the high stimulation frequencies used to induce LTP. Based on this model, we propose that extracellular $Ca^{2+}$ could act in a retrograde manner to modulate presynaptic function through a CaR-dependent mechanism.

## METHODS

### Conceptual framework for the model

The synaptic cleft may be represented by a very thin disk of extracellular fluid, the thickness of which is about twice that of the plasma membrane. Because of the narrowness of the synaptic cleft, we suspected that at high stimulation frequencies the interval between pulses would be insufficient for diffusion of $Ca^{2+}$ from the periphery of the cleft to replace extracellular $Ca^{2+}$ depleted at the center of the cleft as a result of activation of postsynaptic, $Ca^{2+}$-permeable channels. Substantial depletion of extracellular $Ca^{2+}$ (e.g., from 1.6 to 0.8 mM) has been documented in perfused hippocampal slices during electrical stimulation or the application of NMDA, quisqualate, or other glutamate receptor agonists (Arens et al., 1992). These changes in extracellular $Ca^{2+}$ result from $Ca^{2+}$ influx through $Ca^{2+}$-permeable channels. Subsequent removal of the agonists can transiently increase extracellular $Ca^{2+}$ above basal values (i.e., to levels of ~2.2 mM) as a result of transient activation of the $Ca^{2+}$ pump and $Na^+/Ca^{2+}$ exchanger (Arens et al., 1992). Because the density of NMDA and other $Ca^{2+}$-conducting pathways can be higher in postsynaptic membranes than in other areas, activity-dependent changes in extracellular $Ca^{2+}$ within the clefts, especially at higher frequencies of stimulation, could be even greater than those measured previously within intercellular spaces. Because of the difficulty of directly measuring extracellular $Ca^{2+}$ within small extracellular spaces such as the synaptic cleft, we have employed modeling of extracellular $Ca^{2+}$ dynamics within the synaptic cleft as an approach to clarifying the effects of stimulation frequency on extracellular $Ca^{2+}$ during synaptic transmission.

### General description: derivation of the model

The simplified model used in our simulations includes the following morphological elements: the presynaptic membrane, synaptic cleft, and dendritic spine of the postsynaptic neuron. The last contains a head and a neck, which are of variable lengths and radii (Fig. 1). The synaptic cleft represents a cylinder with a height of 15 nm. It contains several concentric rings with variable number and delta radii. The spine head represents the postsynaptic intracellular space where $Ca^{2+}$ accumulates during synaptic activation. Diffusion of calcium within the neck conforms to the geometry of the neck. Cytosolic $Ca^{2+}$ in the dendritic shaft underneath the spine is assumed to stay constant at 50 nM. Parameters for diffusion within the synaptic cleft are based on a cylindrical diffusion equation, where $D$ is based on estimates and experimental data obtained in studies on $D$ in restricted diffusion compartments and narrow extracellular spaces in excitable systems (Hodgkin and Keynes, 1957; Niedergerke, 1957; Kush-

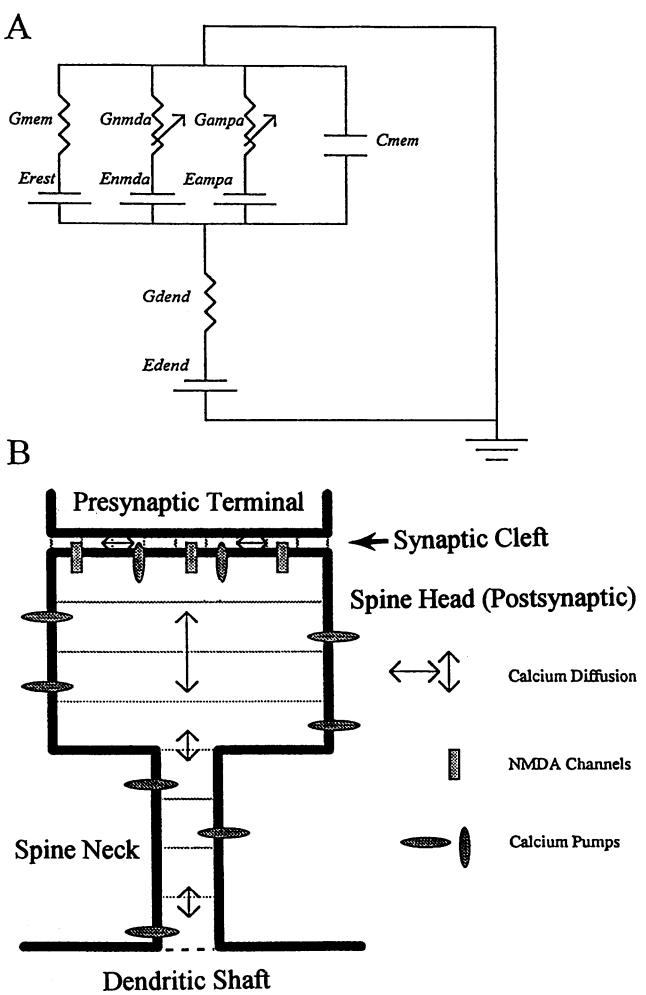


FIGURE 1 Electric equivalent circuit (*A*) and model of $Ca^{2+}$ dynamics (*B*) in synaptic cleft between a presynaptic terminal and a dendritic spine. The boundary between the dendritic shaft and the spine neck is marked with a dashed line. See explanations in the text and meanings of the symbols in Table 1.

merick and Podolsky, 1969; Nasi and Tillotson, 1985; Bers and Peskoff, 1991; Kargacin and Fay, 1991; Kargacin, 1994).

Our simulations (see Results) suggest that the magnitude of the depletion of extracellular $Ca^{2+}$ near the center of the synaptic cleft is large enough to be detected by calcium-sensing receptors. To model these changes in synaptic extracellular $Ca^{2+}$, we have built upon a model developed by Zador et al. (1990) of the internal calcium dynamics in dendritic spines. This model includes calcium influx from the synaptic cleft into the head of the spine through NMDA channels and efflux through calcium pumps and $Na^+/Ca^{2+}$ exchangers. Concentrations of extracellular $Ca^{2+}$ inside the cleft are estimated by using a compartmental model incorporating flux across the postsynaptic membrane and radial diffusion from the edges of the cleft.

## Electric circuit model

The flux of calcium ions through NMDA channels is determined by electrodiffusion forces described by the Goldman-Hodgkin-Katz equations, which are dependent upon membrane potential. To model the membrane potential, we simulate an equivalent circuit of the spine head (depicted in Fig. 1 *A*), which includes three current sources: α-amino-3-hydroxy-5-methylisoxazole-4-propionic acid (AMPA)/kainate channels, NMDA channels, and current from the dendritic shaft. An estimate of synaptic currents after the release of glutamate into the synaptic cleft is given in the model of Zador et al. (1990). The time course of AMPA current, $I_{ampa}$, upon glutamate release at time $t = 0$ is given as

$$I_{ampa}(t) = (E_{ampa} - V_{mem})g_{ampa}\frac{e}{t_{peak}}t\exp\left(-\frac{t}{t_{peak}}\right), \quad (1)$$

where $V_{mem}$ is the spine head potential, $E_{ampa}$ is the reversal potential of AMPA channels, $g_{ampa}$ is the maximum conductance of AMPA channels for a single spike, $t_{peak}$ is the time of the peak conductance, and $e$ is the natural logarithm. The model also includes the time course of NMDA current, $I_{nmda}$, with a double exponential form as well as the nonlinear voltage dependence due to magnesium-mediated blockade, given as

$$I_{nmda}(t) = (E_{nmda} - V_{mem})g_{nmda}\frac{\exp(-t/\tau_1) - \exp(-t/\tau_2)}{1 + \eta\cdot[Mg^{2+}]_o\cdot\exp(-\gamma V_{mem})}, \quad (2)$$

where $E_{nmda}$ is the reversal potential of NMDA channels, $g_{nmda}$ is the maximum conductance of NMDA channels for a single spike, $\tau_1$ is the channel closing time, $\tau_2$ is the channel opening time, $\eta$ is the prefactor of $Mg^{2+}$ block, and $\gamma$ is the voltage factor of $Mg^{2+}$ block (see Table 1). These equations for synaptic currents describe the time course of the conductance change resulting from many postsynaptic membrane channels being open after glutamate release by a single presynaptic spike.

Holmes and Levy (1990) have argued that for multiple-spike models, at any given time only a small fraction of the total population of channels are active, in which case saturation effects can be neglected and the net conductance time course can be considered as the sum of the individual time courses for each spike. Their suggestion is based on the observation that NMDA channels play a less significant role in depolarization than AMPA channels. Modeling indicates that because NMDA channels have a higher conductance and longer mean open time than AMPA channels, and because they have been observed in equal numbers in the postsynaptic membrane, to explain their less significant role in depolarization, a smaller fraction of them must be active. Adopting this assumption, for most of our simulations we neglected saturation effects and modeled the net conductance as the sum of the individual conductance time courses. In additional simulations (Fig. 3) we also considered an alternative case in which the activation of a population of channels can be saturated by the release of glutamate caused by a single presynaptic spike. In this case, the higher net conductance value resulting from summation of individual conductance time courses is fixed to the maximum conductance ($g_{mmda}$, $g_{ampa}$) for a single spike.

The spine head potential is also determined by a current due to leakage from a depolarized dendrite. To produce significant depolarization in the dendrite, a large number of synaptic sites must be active simultaneously. The currents from a single synapse on a spine head, which may yield strong depolarization at the spine head, may not cause substantial depolarization

**TABLE 1 Symbols, units, and default parameter values used in the computer simulations**

| | | |
|---|---|---|
| Spine geometry | | |
| Radius of spine head | | 250 nm |
| Length of spine head | | 500 nm |
| Radius of spine neck | | 50 nm |
| Length of spine neck | | 700 nm |
| Gap of synaptic cleft | | 15 nm |
| Compartment sizes | | |
| Radial size in cleft | | 10 nm |
| Axial length in spine | | 100 nm |
| Ionic concentrations | | |
| $[Ca^{2+}]_o$ | External calcium | 1.5 mM |
| $[Ca^{2+}]_i$ | Internal calcium | 50 nM |
| $[Mg^+]_o$ | External magnesium | 1.2 mM |
| $[M^+]$ | Monovalent ions | 150 mM |
| Diffusion constants | | |
| $D_{spine}$ | $Ca^{2+}$ in cytoplasm | $6.0 \times 10^{-6}$ cm²/s |
| $D_{cleft}$ | $Ca^{2+}$ in cleft | $0.3 \times 10^{-6}$ cm²/s |
| Electric circuit parameters | | |
| $C_{mem}$ | Membrane capacitance | 1 μF/cm² |
| $R_{mem}$ | Membrane resistance | 30 kΩ cm² |
| $E_{rest}$ | Resting potential | −70 mV |
| $R_{axial}$ | Axoplasmic resistance | 100 Ω cm |
| $E_{dend}$ | Dendrite potential | −45 mV |
| AMPA channels | | |
| $E_{ampa}$ | Reversal potential | 0 mV |
| $g_{ampa}$ | Maximum conductance | 0.5 nS |
| $t_{ampa}$ | Channel closing time | 1.5 ms |
| NMDA channels | | |
| $E_{nmda}$ | Reversal potential | 0 mV |
| $g_{nmda}$ | Maximum conductance | 0.2 nS |
| $\tau_1$ | Channel closing time | 80 ms |
| $\tau_2$ | Channel opening time | 0.67 ms |
| $\eta$ | Prefactor of magnesium block | 0.33/mM |
| $\gamma$ | Voltage factor of magnesium block | 0.06/mV |
| $P_{ca}/P_m$ | Calcium permeability ratio | 3.2:1 |
| Calcium efflux pathways | | |
| $P_sK_{max}$ | Pump efficiency, ATPase | $1 \times 10^{-15}$ μmol/(ms μm²) |
| $P_sK_{max}$ | Na/Ca exchange efficiency | $5 \times 10^{-15}$ μmol/(ms μm²) |
| $K_d$ | Pump affinity, ATPase | 0.5 μM |
| $K_d$ | Na/Ca exchange affinity | 20 μM |
| Calcium buffers | | |
| $B_{total}$ | Concentration of buffering sites | 120 μM |
| $k_f$ | Forward buffering rate | 0.5 μm/ms |
| $k_r$ | Backward buffering rate | 0.5/ms |

in the dendrite. This is because, due to its larger geometry, the dendrite has a capacitance several orders of magnitude larger than that of the spine head and thus requires larger currents to change its potential. The dendrite behaves approximately like a battery with respect to a single spine, because its voltage remains relatively constant despite fluctuations in the spine's potential. Previous studies (Zador et al., 1990; Schiegg et al., 1995) have modeled the depolarization of the dendrite by considering large numbers of coactive synaptic inputs on the dendrite. The key feature of this modeling is that it produces significant depolarizations in the dendrite, which leak into the spine head, reducing the magnesium-induced blockade of NMDA channels. Instead of modeling multiple synaptic sites, we have chosen to treat the dendrite as a battery, with its potential reflecting the degree of coactive synaptic input. The dendrite voltage is clamped and connected to the spine head by an axial conductance characteristic of the spine neck. The current sources as well as membrane capacitance, leakage conductance, and resting potential are incorporated into a circuit model giving the spine head's membrane potential as

$$\frac{dV_{mem}}{dt} = \frac{1}{C_{mem}}[I_{ampa}(t) + I_{nmda}(t) + g_{neck}(E_{dend} - V_{mem}) + g_{mem}(E_{rest} - V_{mem})], \quad (3)$$

where $I_{ampa}(t)$ and $I_{nmda}(t)$ are defined as above, $E_{dend}$ is the clamped dendrite voltage, $g_{neck}$ is the conductance through the spine neck, $E_{rest}$ is the resting potential, $g_{mem}$ is the resting membrane conductance, and $C_{mem}$ is the membrane capacitance. The parameters $C_{mem}$, $g_{mem}$, and $g_{neck}$ depend upon the spine geometry. They are computed for each spine geometry from estimates of membrane capacitance ($\mu$F/cm$^2$), membrane resistance (k$\Omega$ cm$^2$), and axoplasmic resistance ($\Omega$ cm) as given by $C_m$, $R_m$, and $R_{axial}$, respectively, in Table 1.

## Calcium flux through NMDA channels

A significant portion of the current passing through the NMDA channel is due to calcium. Zador et al. (1990) neglected electrodiffusion effects (Qian and Sejnowski, 1989) and assumed that the calcium current is some fraction of the net NMDA current. This should be a valid assumption as long as either of two criteria is met: 1) the internal and external ionic concentrations are not changed substantially, or 2) the membrane voltage remains substantially below the reversal potential, $E_{nmda}$. In our simulations we considered substantial changes in both internal and external concentrations and a variety of membrane voltages. Thus it was necessary to incorporate electrodiffusion effects described by the Goldman-Hodgkin-Katz (GHK) current equation. Schneggenburger et al. (1993) use the GHK equation to derive an expression for the fraction of current, $P_f$, through the NMDA channel that is due to calcium as a function of membrane voltage and ionic concentrations. We adopt their expression, with the exception that we do not follow their assumption that internal calcium concentrations are negligible:

$$P_f = \frac{I_{Ca}}{I_M + I_{Ca}} = \left\{1 + \frac{P_m[M^+](1 - \exp(2FV_{mem}/RT))}{4P_{ca}([Ca^{2+}]_o - [Ca^{2+}]_i \exp(2FV_{mem}/RT))}\right\}^{-1}. \quad (4)$$

In this expression $I_{Ca}$ and $I_{M+}$ are the calcium and monovalent ionic currents, respectively; $M^+$ represents positively charged monovalent ionic concentrations; $P_m$ is the GHK permeability to monovalent ions; $P_{ca}$ is the GHK permeability to calcium ions; $V_{mem}$ is the spine head potential; and $F$, $R$, and $T$ have their usual thermodynamic meanings. As in the derivation of Schneggenburger et al. (1993), it is assumed that internal and external concentrations of monovalent ions are nearly equal and do not change significantly during stimulation. A recent estimate for the permeability ratio $P_{ca}/P_m$ for the NMDA channel is given as 3.6:1 by Spruston et al. (1995). Because the reversal potential depends on the concentration of different ions, we also recompute the reversal potential, $E_{nmda}$ in Eq. 2, as given by the GHK voltage equation:

$$E_{nmda} = \frac{2F}{RT}\log\left(\frac{(P_m/P_{Ca})[M^+]_o + 4[Ca^{2+}]_o}{(P_m/P_{Ca})[M^+]_i + 4[Ca^{2+}]_i}\right). \quad (5)$$

The expression for calcium current becomes indeterminant when the membrane potential is at the reversal potential, so some care must be taken in evaluating it numerically. With the update of Eq. 5, the product of the fraction $P_f$ and the NMDA current given in Eq. 2 provides an estimate of the calcium current through NMDA channels over a wide range of voltages and concentrations.

One final modification is necessary to convert this calcium current into a calcium flux. The conductance $g_{nmda}$ in Eq. 2 is an estimate for the entire synapse. For the case of an individual compartment in the model of the cleft, the current calculated from this conductance will be too large, because it is representative of the entire synapse and not the limited region that the compartment represents. Assuming that the NMDA channels are distributed uniformly in the postsynaptic membrane, the conductance should be scaled in proportion to the fraction of membrane represented by that compartment. However, because conversion from current to flux involves scaling that is inversely proportional to the volume, the expression for the calcium flux of a compartment in the cleft is simplified as

$$\frac{\partial[Ca^{2+}]_o}{\partial t} = \frac{P_f \cdot (I_{nmda} \cdot A_{frac})}{2F(V_o \cdot A_{frac})} = -\frac{P_f \cdot I_{nmda}}{2FV_o}, \quad (6)$$

where the valence of the ions is $2e$, as reflected by the term in the denominator; $F$ is Faraday's constant ($9.649 \times 10^{13}$ coulomb/mM); $P_f$ and $I_{nmda}$ are computed as dictated in Eqs. 2, 4, and 5 for the compartment under consideration; $A_{frac}$ is the fraction of the cleft that the compartment represents; and $V_o$ is the volume of the entire synaptic cleft.

## Calcium efflux pathways

The model includes two calcium extrusion pathways, each of which follows the Michaelis-Menten kinetics given in Zador et al. (1990):

$$\frac{\partial[Ca^{2+}]_o}{\partial t} = -\frac{A}{V}\left\{G_{leak}([Ca^{2+}]_o - [Ca^{2+}]_i) - P_s K_{max}\frac{[Ca^{2+}]_i}{[Ca^{2+}]_i + Kd}\right\}, \quad (7)$$

where $A/V$ is the ratio of membrane surface area to the volume of the compartment under consideration. CaATPase has a low capacity ($P_sK_{max} = 1 \times 10^{-15}$ $\mu$M/ms $\mu$m$^2$) but a high affinity, i.e., it operates at low calcium concentrations ($K_d = 0.5$ $\mu$M), whereas the Na/Ca exchanger has a high capacity ($P_sK_{max} = 5 \times 10^{-15}$ $\mu$M/ms $\mu$m$^2$) but a low affinity ($K_d = 20$ $\mu$M). Because there are few data concerning their densities, values for their efficiencies are chosen to keep the model in agreement with experimental results. These values for pump efficiencies are larger than those used by Zador et al. (1990), because recent estimates of the NMDA channel's permeability to calcium are larger and thus cause a larger calcium influx, which must be balanced by a higher pump capacity to maintain agreement with experimental results (Schiegg et al., 1995). The leakage conductance, $G_{leak}$, of each pump is set such that there is no net calcium current at resting concentrations.

## Calcium buffering

Calmodulin (CaM) buffers the internal calcium concentration. It has four $Ca^{2+}$-binding sites per molecule, which are bound sequentially. The effects from sequential binding have been neglected, with the simplification that

each binds independently. The concentration of calmodulin has been estimated as 30 $\mu$M (Carafoli, 1987). Because binding sites are approximated as functioning independently, the concentration is taken as four times greater, or 120 $\mu$M. The rate equation for the buffer and calcium concentrations is given as

$$\frac{\partial[Ca^{2+}]_i}{\partial t} = \frac{\partial[B_{free}]}{\partial t} = k_f[Ca^{2+}]_i[B_{free}] + k_r([B_{total}] - [B_{free}]), \quad (8)$$

where $B_{total}$ is the total concentration of buffer binding sites, $B_{free}$ is the concentration of unbound sites, and $k_f$ and $k_r$ are the forward and backward rate constants. We adopt parameter values, $k_f = 0.5$ $\mu$M/ms and $k_r = 0.5$ $ms^{-1}$, as used by Schiegg et al. (1995). Because the diffusion of calmodulin is slow relative to that of calcium, it has been neglected and the buffer is assumed to be immobile.

## Axial diffusion in the spine

The spine is modeled with two connected cylinders, one representing the head (length 300 nm, radius 250 nm) and the second representing the neck (length 700 nm, radius 50 nm). To model axial diffusion, the spine is discretized into compartments, each 100 nm in length. The distribution of flux sources in the compartmental model is depicted in Fig. 1 *B*. NMDA channels are only located within the synaptic cleft and therefore only affect the top compartment of the spine head. Calcium efflux entities are assumed to be uniformly distributed throughout the plasma membrane of the head and neck. Furthermore, the concentration of calmodulin is assumed to be uniform throughout the cytoplasm of the head and the neck. Last, as a boundary condition in modeling, it is assumed that $Ca_i$ within the dendritic shaft is fixed at resting levels similar to those of other models of the spine (Zador et al., 1990; Schiegg et al., 1995).

At the topmost shell of the spine head, calcium enters through NMDA channels and is extruded by calcium efflux pathways. To compute the calcium flux into the top shell, we first define the flux for each compartment of the synaptic cleft, $F(Ca^{2+}, r, t)$, as the sum of the fluxes from Eqs. 6 and 7. Then we compute the net flux into the top shell as

$$\frac{\partial[Ca^{2+}]_i}{\partial t} = -\frac{V_o}{V_s}\left\{\frac{\int F(Ca^{2+}, r, t) r\, dr}{\int r\, dr}\right\}, \quad (9)$$

where the integration is performed from the center of the cleft to the edge, $V_o$ is the volume of the cleft, and $V_s$ is the volume of the topmost shell. Because NMDA channels can open only when glutamate is released in high concentrations in the synaptic cleft, the flux due to NMDA channels is only considered at the top of the spine head. Flux due to calcium pumps is considered on all regions of the spine's membrane. This efflux is given by Eq. 7 when its sign is reversed, and the ratio $A/V$ is chosen for the ratio of membrane area to volume for a spine compartment instead of a cleft compartment. These sources of flux are added to the flux due to calcium buffering as defined in Eq. 8, to give the net calcium flux in each spine compartment, $F(Ca^{2+}, z, t)$.

For modeling diffusion of calcium within the spine, we have neglected diffusion in the radial direction, focusing on axial diffusion from the top of the spine head down through the neck to the dendrite. Diffusion in the axial direction is described as

$$\frac{\partial[Ca^{2+}]}{\partial t} = D_{spine}\frac{\partial^2[Ca^{2+}]}{\partial z^2} + F(Ca^{2+}, z, t), \quad (10)$$

where $D_{spine}$ is the diffusion constant of $Ca^{2+}$ in cytoplasm. The key advantage to neglecting radial diffusion within the spine is that an implicit integration technique (the Crank-Nicolson method) can be easily applied to diffusion along one dimension (Crank and Nicolson, 1947; Crank, 1975; Mascagny, 1989). This technique is more stable than the forward Euler technique, and thus permits the use of larger time steps, allowing much faster simulations (Mascagny, 1989).

## Radial diffusion in the cleft

The synaptic cleft is modeled as a flat cylindrical shell above the spine head (height 15 nm). Calcium flux into the spine head through NMDA channels leads to a depletion of extracellular $Ca^{2+}$ within the cleft. We neglect diffusion in the vertical direction of the cleft because of its narrowness and consider only radial diffusion from the edges to the center. Ion concentrations at the edges of the cleft are assumed to be fixed at external resting levels. The equation for radial diffusion is given as

$$\frac{\partial[Ca^{2+}]}{\partial t} = \frac{1}{r}\frac{\partial}{\partial r}\left(rD_{cleft}\frac{\partial[Ca^{2+}]}{\partial r}\right) + F(Ca^{2+}, r, t), \quad (11)$$

where $r$ is the radial distance from the center of the cleft, $D_{cleft}$ is the diffusion constant within the cleft, and $F(Ca^{2+}, r, t)$ is defined as in Eq. 9.

The calcium flux, $F(Ca^{2+}, r, t)$, is caused by NMDA channels and calcium efflux pathways. It depends on several factors: activation of NMDA channels by glutamate, the membrane potential, the cytosolic $Ca^{2+}$ inside the spine, and the extracellular $Ca^{2+}$ within the cleft. Although glutamate is randomly released in discrete packets within the cleft, we consider its average effect over time with the simplification that it is spread uniformly across the cleft, i.e., that the activation of NMDA channels from a synaptic event within the cleft is uniform. Recent modeling suggests that glutamate released from vesicles may diffuse rapidly through the cleft, achieving a relatively uniform distribution in a short time (Clements, 1990). However, these estimates do not include binding to channels on the postsynaptic membrane, which may limit its spread. In future modeling we may consider these dynamics. If the activation of NMDA channels is nonuniform, it will be necessary to model diffusion in the cleft with a planar grid as opposed to concentric rings. Likewise, it will also be necessary to model diffusion in the plane parallel to the cleft inside the spine head. The advantage of the current model has been that the radial diffusion in the cleft and axial diffusion in the spine occur along one dimension, which makes possible the application of implicit integration techniques that have commonly been used in modeling electrical propagation in cables.

# RESULTS

## Application of the model to estimate frequency-dependent changes in extracellular $Ca^{2+}$

To explore the frequency dependence of $Ca^{2+}$ dynamics within the synaptic cleft, the profiles of the changes in extracellular $Ca^{2+}$ at various distances from the center of the cleft were modeled as a function of the frequency of stimulation. Fig. 2 illustrates the results of these simulations when the values of the free parameters were assumed to be similar to those used in previous models of the spine (Zador et al., 1990; Schiegg et al., 1995) (see Table 1). At a low frequency of stimulation (3 Hz) (Fig. 2 *A*), the first pulse causes an initial drop in extracellular $Ca^{2+}$ at the center of the cleft from 1.5 to approximately 1.39 mM, because of $Ca^{2+}$ influx through activated NMDA channels. During the 333-ms interval between pulses, extracellular $Ca^{2+}$ returns to its basal level because of $Ca^{2+}$ diffusion from the periphery toward the center of the cleft as well as $Ca^{2+}$ efflux across the postsynaptic membrane mediated by the $Ca^{2+}$ pump and $Na^+/Ca^{2+}$ exchanger. The next stimulus starts from the original basal level and causes the same initial change in extracellular $Ca^{2+}$ (Fig. 2 *A*). With a slightly higher frequency of stimulation (5 Hz), however, the interpulse interval is not long enough for extracellular $Ca^{2+}$ to

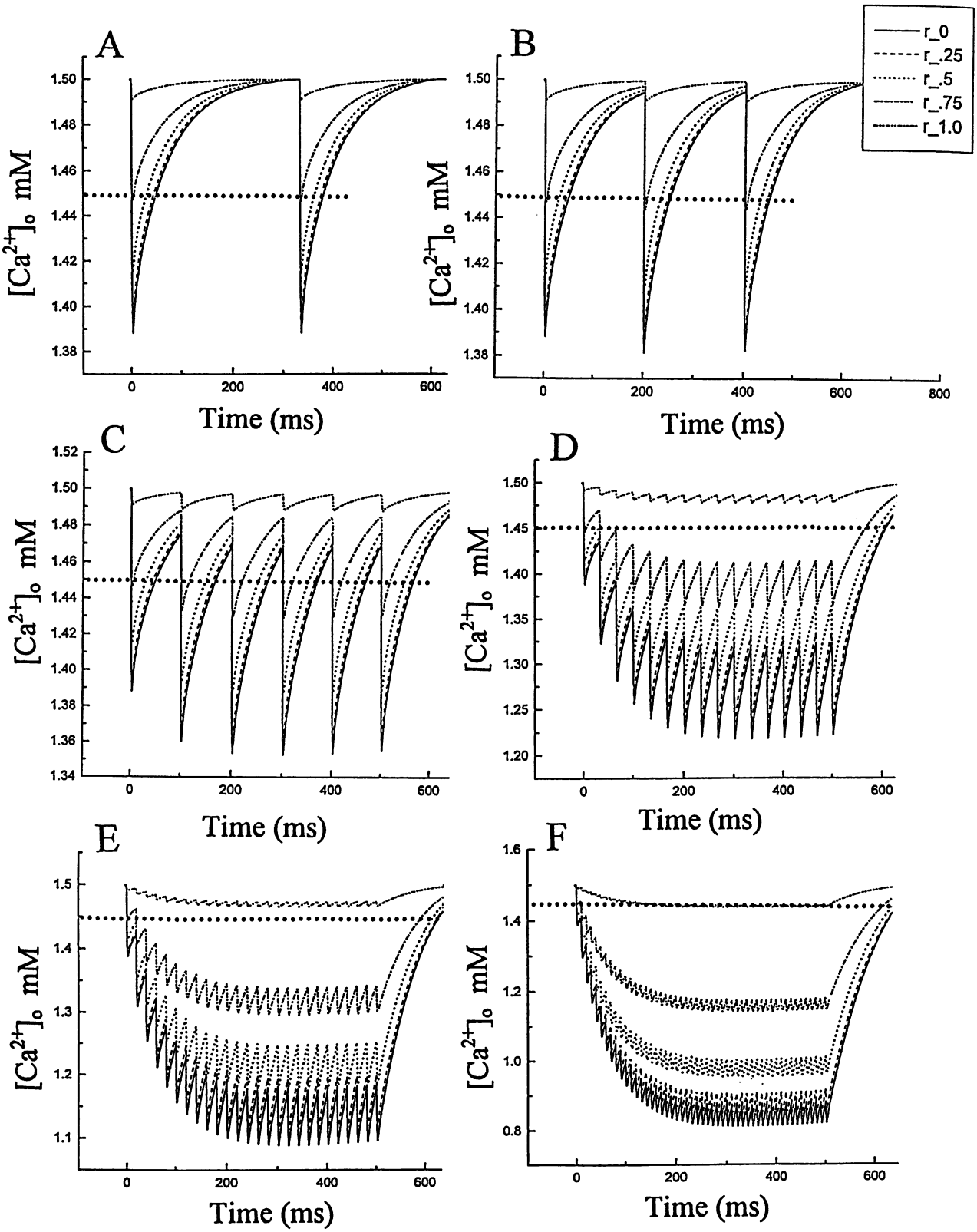


FIGURE 2 Time course for changes in $Ca^{2+}$ concentration in the synaptic cleft at different stimulation frequencies: 3 Hz in *A*; 5 Hz in *B*; 10 Hz in *C*; 30 Hz in *D*; 50 Hz in *E*; and 100 Hz in *F*. The profiles of extracellular $Ca^{2+}$ changes at different distances from the center of the cleft are marked with different lines, as indicated in the insets. The center is marked with r_0 and the periphery with r_1.0. Other lines: r_.25, r_.5, and r_.75 indicate 25%, 50%, and 75% of the distance from the center to the periphery of the cleft, respectively. Default values were used for the other parameters, as shown in Table 1.

return to its basal level, and the second stimulus starts from a lower initial level of extracellular $Ca^{2+}$ and, therefore, produces a more substantial depletion of extracellular $Ca^{2+}$ in the cleft (Fig. 2 *B*). This effect becomes more pronounced at higher frequencies (Fig. 2 *C–D*), resulting in substantial extracellular $Ca^{2+}$ depletion, to a level of approximately 0.8 mM at 100 Hz (Fig. 2 *F*). At this frequency, more than 20 pulses are necessary to reach the maximum depletion of extracellular $Ca^{2+}$, which is then maintained during subsequent stimulations.

For these simulations saturation effects involving a defined population of active channels were ignored, as justified in Materials and Methods. Fig. 3 shows, however, that even when they have been taken into consideration, i.e., when the net conductance resulting from summation of individual conductance time courses is fixed to the maximum conductance for a single presynaptic spike, a reduction in the extracellular $Ca^{2+}$ level in the synaptic cleft to approximately 1.38 mM occurs at 100 Hz.

## Effect of varying the diffusion coefficient for cytosolic $Ca^{2+}$ on the simulations

The simulations in Fig. 2 indicate that at frequencies higher than 10–30 Hz, the interpulse intervals are too short for extracellular $Ca^{2+}$ to return to its original basal level, resulting in reductions in extracellular $Ca^{2+}$ at stimulations

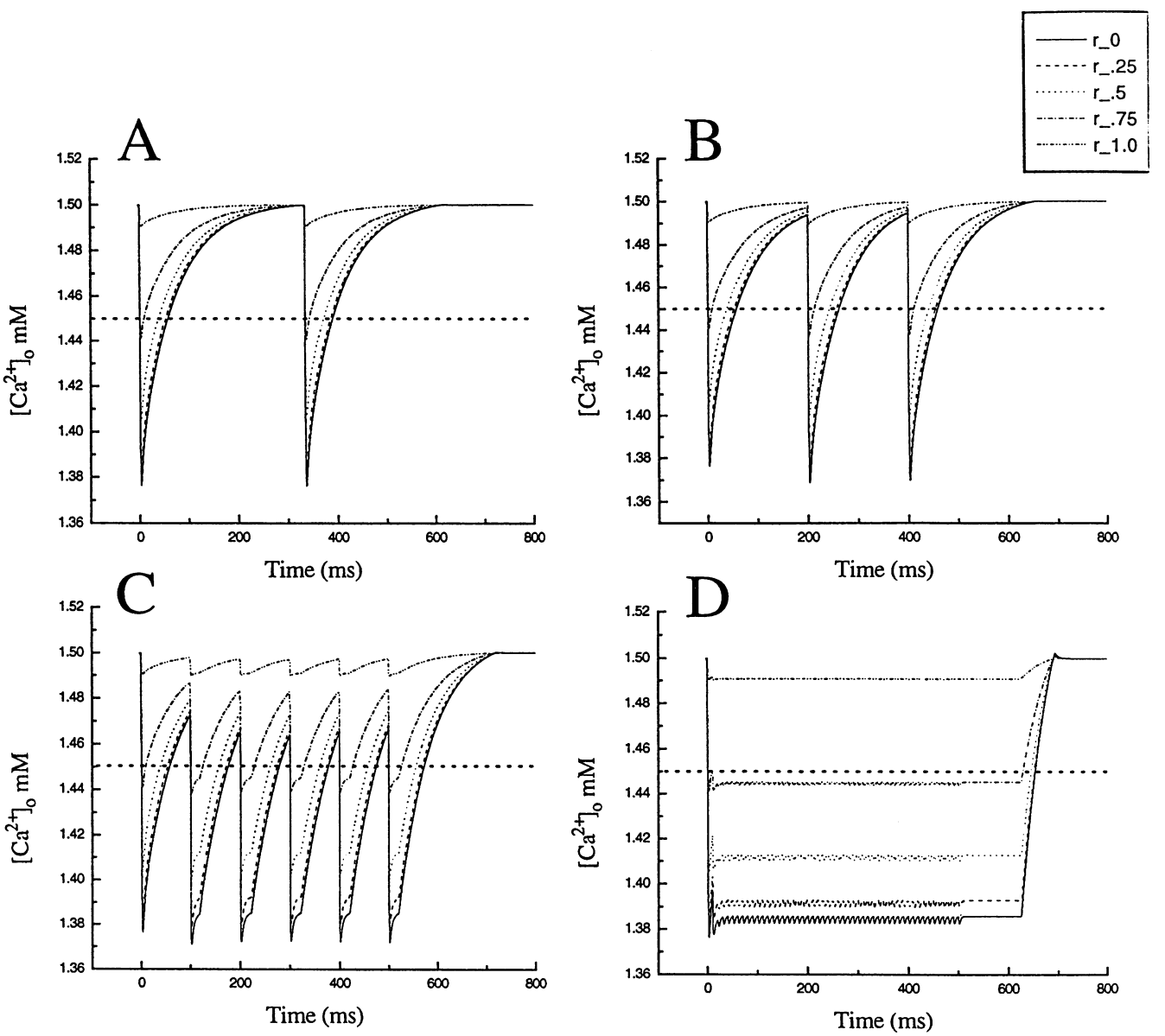


FIGURE 3 Time course for changes in extracellular $Ca^{2+}$ in the cleft with consideration of saturation effects mediated by a single spike. The net conductance value is fixed to the maximum conductance ($g_{nmda}$, $g_{ampa}$) for a single spike. The stimulation frequencies are 3 Hz in *A*; 5 Hz in *B*; 10 Hz in *C*; and 100 Hz in *D*. The other conventions are as described in Fig. 2.

longer than 100–300 ms that occur mainly because of restricted diffusion of $Ca^{2+}$ from the periphery to the center of the cleft. It is difficult to estimate precisely the diffusion coefficient for $Ca^{2+}$ within the cleft, but it is probably smaller than the range of values reported for restricted diffusion spaces, including extracellular compartments of transverse tubules ($0.14–1.2 \times 10^{-6}$ $cm^2/s$) (Hodgkin and Keynes, 1957; Niedergerke, 1957; Kushmerick and Podolsky, 1969; Nasi and Tillotson, 1985; Bers and Peskoff, 1991; Kargacin, 1994), because the synaptic gap is extremely narrow and may be filled with extracellular macromolecular components that could act as a substantial diffusion barrier for $Ca^{2+}$. For most of the simulations we have utilized a value within this range, $0.3 \times 10^{-6}$ $cm^2/s$. From the simulations shown in Fig. 4, however, it can be seen that at larger values of $D$(Ca), a substantial depletion of extracellular $Ca^{2+}$ can also occur at high frequencies. Even at $1.0 \times 10^{-6}$ $cm^2/s$, stimulation at 100 Hz induces a reduction of extracellular $Ca^{2+}$ from 1.5 to 1.22 mM.

## Effects of varying the geometry of the synaptic cleft and spine on the simulations

We have also examined the effects of varying the geometrical parameters of the cleft. Although the width of the cleft is relatively invariant and is generally reported to be 15 nm (Sudhof, 1995), we also performed simulations assuming a twofold larger value, 30 nm (Fig. 5 *A*). Under this condition, extracellular $Ca^{2+}$ was also reduced to less than 1.1 mM at a high stimulation frequency (100 Hz). The dendritic spines can also vary in size (Harris and Stevens, 1989; Shepherd, 1996). A slightly less pronounced extracellular $Ca^{2+}$ depletion occurred at 100 Hz when the head length was reduced (Fig. 5 *B*) or the neck radius was increased (Fig. 5 *D*), whereas opposite effects were observed in spines modeled with a longer neck (Fig. 5 *C*) or smaller neck radius (Fig. 5 *E*).

## Dependence on membrane potential and ion permeability ratios

Changes in the potential across the postsynaptic membrane could also contribute to extracellular $Ca^{2+}$ dynamics in the cleft, because of the voltage dependence of the block of NMDA channels by $Mg^{2+}$ (Ascher et al., 1988; Bliss and Collingridge, 1993). The decrease in extracellular $Ca^{2+}$ is more pronounced at potentials of −30 to −10 mV (Fig. 6 *A–C*) than at −60 mV (Fig. 6 *D*), as a result of the removal of $Mg^{2+}$ blockade at voltages above the threshold values. This effect was smaller at −10 mV (Fig. 6 *A*) than at −20 (Fig. 6 *B*) and −30 mV (Fig. 6 *C*), because of the reduction in the electrochemical driving forces.

Different values for permeability ratios ($P_{ca}/P_m$) of NMDA receptor channels have been reported (Dudek and Baer, 1992; Rogers and Dani, 1995; Spruston et al., 1995). In most of the simulations (Fig. 2) we have used a ratio of 3.2:1, similar to that measured previously (Spruston et al., 1995). For comparison, we made an assessment at a much lower ratio, 0.5:1 (Fig. 6 *E*), but even at this value the extracellular $Ca^{2+}$ level was reduced to approximately 1.32 mM at 100 Hz. In recent studies much higher values for this parameter have been reported (Dudek and Baer, 1992; Rogers and Dani, 1995). It was found that under defined conditions, NMDA channels can be 13 times more permeable for $Ca^{2+}$ than for monovalent cations (Rogers and Dani, 1995). The simulation at a similar ratio, $P_{ca}/P_m$ =

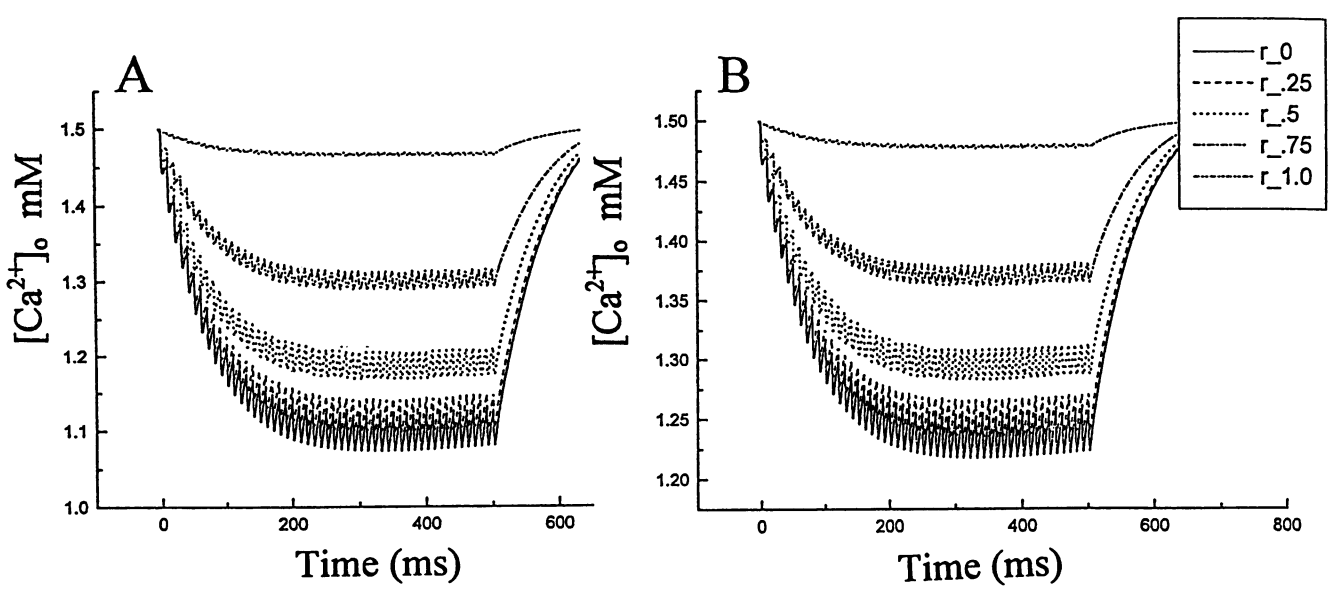


FIGURE 4 Changes in extracellular $Ca^{2+}$ in the synaptic cleft induced by a 100-Hz train of stimuli at different diffusion coefficients ($D_{cleft}$): $0.6 \times 10^{-6}$ $cm^2/s$ in *A* and $1.0 \times 10^{-6}$ $cm^2/s$ in *B*. The lines marked in the insets are the same as described in Fig. 2. Default values were used for all other parameters (see Table 1).

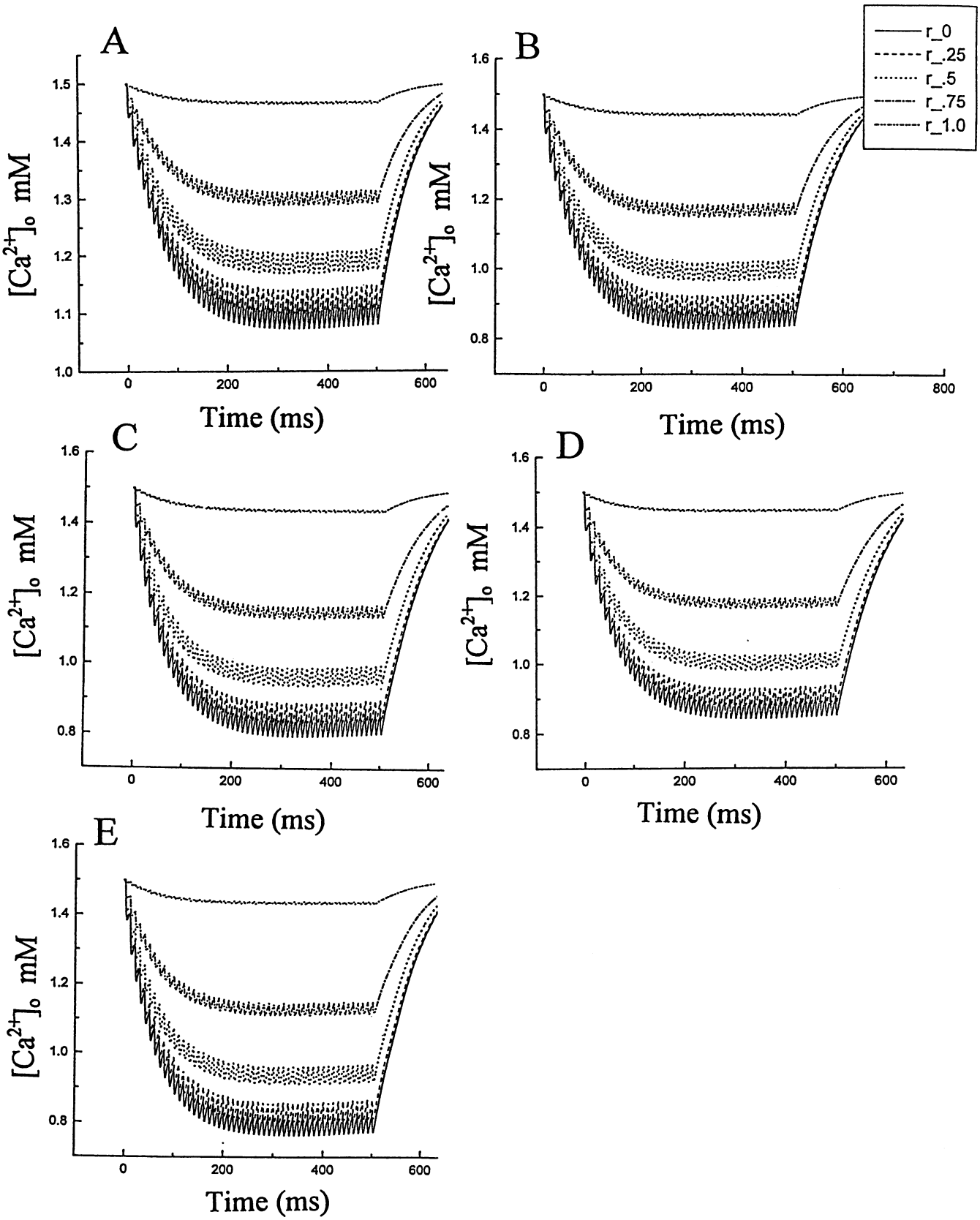


FIGURE 5 Extracellular $Ca^{2+}$ dynamics at 100 Hz in the synaptic cleft and spine with different geometrical parameters: 30-nm cleft gap in *A*; 300-nm length of the spine's head in *B*; 1000-nm length of the neck in *C*; 80-nm radius of the neck in *D*; and 30-nm radius of the neck in *E*.

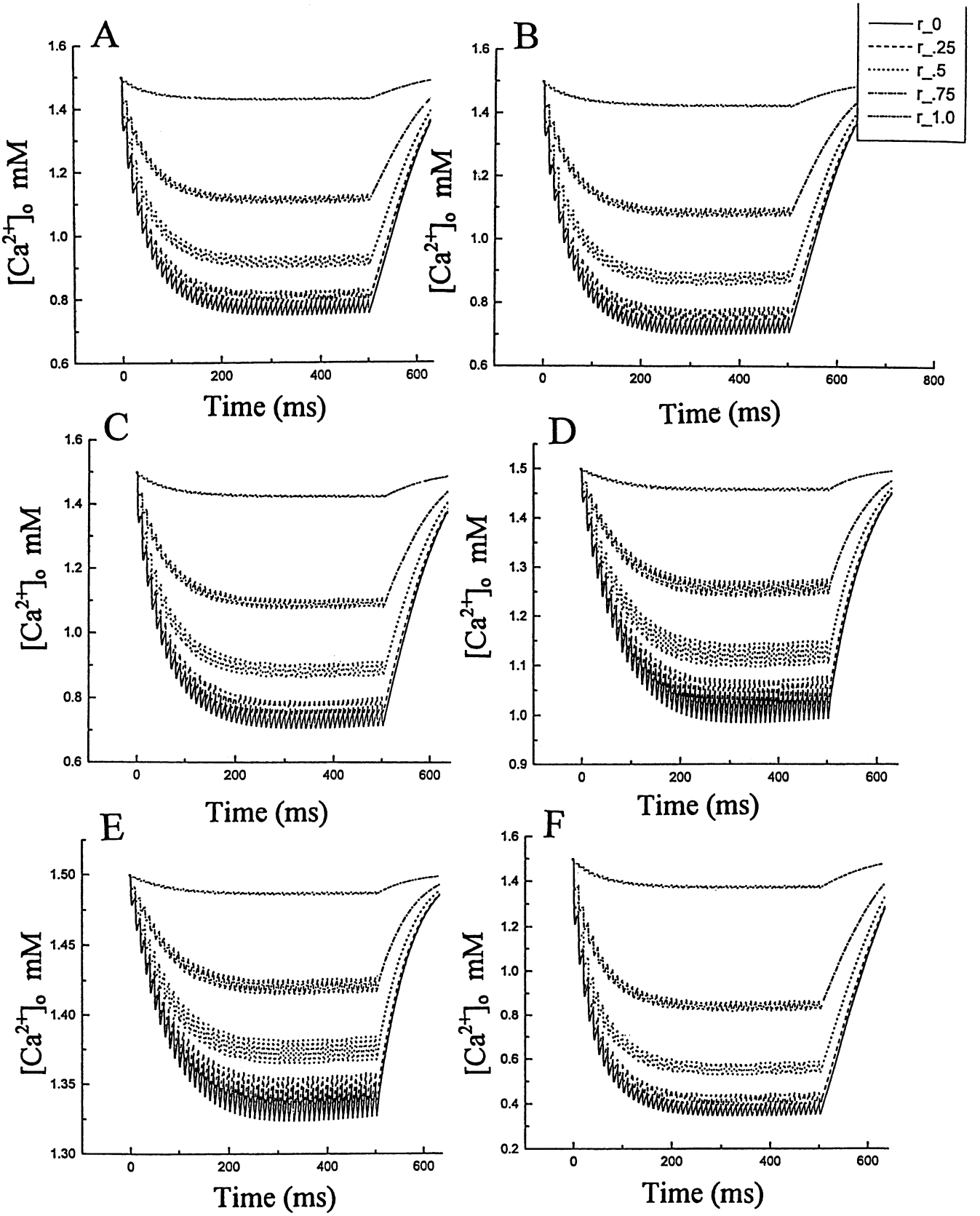


FIGURE 6 Dependence of extracellular $Ca^{2+}$ dynamics in the cleft on membrane potential (−10 mV in *A*; −20 mV in *B*; −30 mV in *C*; and −60 mV in *D*) as well as on the permeability ratio ($P_{ca}/P_m$) for NMDA channels (1:2 in *E*, and 10:1 in *F*).

10:1, revealed a drastic reduction in the level of extracellular $Ca^{2+}$ from 1.5 to 0.35 mM at 100 Hz (Fig. 6 *F*), suggesting that under defined conditions, extracellular $Ca^{2+}$ depletion in the synaptic cleft can be very substantial and its functional implications should be taken carefully into consideration.

### Spatial distribution and average depletion of extracellular $Ca^{2+}$ at different times in the cleft

The average depletion of extracellular $Ca^{2+}$ in the synaptic cleft and its radial distribution at three different times (75 ms, 150 ms, and 300 ms) are shown in Fig. 7, *A* and *B*, respectively. These simulations show that 75 ms after the beginning of stimulation at 100 Hz, the average extracellular $Ca^{2+}$ across the cleft is reduced from 1.5 to approximately 1.2 mM, whereas extracellular $Ca^{2+}$ at the center of the cleft drops to a level lower than 1.0 mM. More pronounced depletions of extracellular $Ca^{2+}$ are observed at 150 ms and 300 ms, reaching a level of less than 0.8 mM in the latter case. The extracellular $Ca^{2+}$ depletion effect augments exponentially from the edge to the center of the synaptic cleft (Fig. 7 *B*).

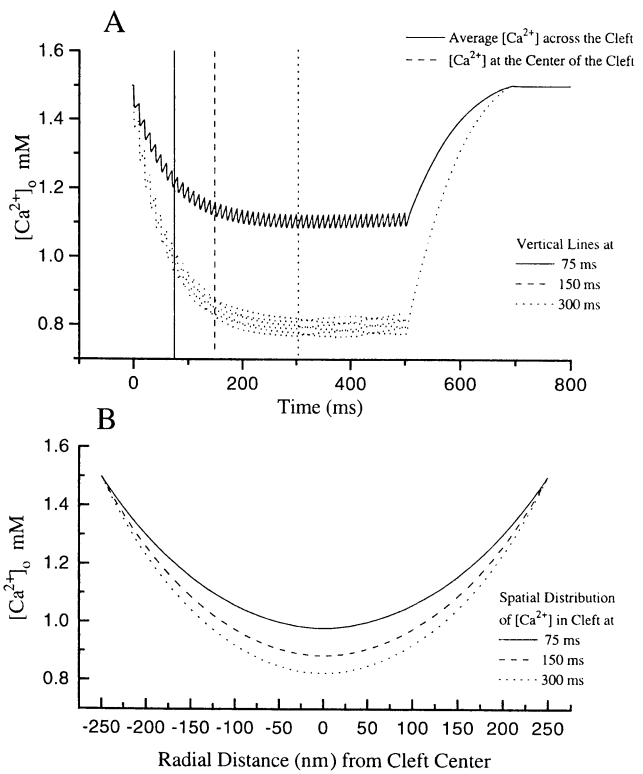


FIGURE 7 Average extracellular $Ca^{2+}$ depletion (*A*) and profiles of spatial distribution of changes in extracellular $Ca^{2+}$ in the synaptic cleft at three different times (*B*) marked in the lower right corner of each panel. The stimulation frequency is 100 Hz.

## DISCUSSION

The results of our simulations with the physiological parameters that we utilized for the synaptic cleft and spine predict that $Ca^{2+}$ influx into the spine via NMDA channels will lead to transitory decreases in extracellular $Ca^{2+}$ within the cleft, which will be larger at high frequencies of stimulation, with reductions reaching 0.8–1.0 mM extracellular $Ca^{2+}$ at 100 Hz. Similar reductions in extracellular $Ca^{2+}$ have been observed in previous studies on perfused hippocampal slices using $Ca^{2+}$-sensitive electrodes during electrical stimulation and application of NMDA and other glutamate receptor agonists (Hamon and Heinemann, 1986; Arens et al., 1992; Lucke et al., 1995). The analytical model in the present study mainly assessed the contribution of NMDA channels, based on available evidence that it is the dominant contributor to postsynaptic $Ca^{2+}$ influx within synapses of the CA1 region of hippocampus (Bliss and Collingridge, 1993). It is likely that more substantial extracellular $Ca^{2+}$ depletion within the synaptic cleft would take place if other $Ca^{2+}$ conductances were added to our model, such as voltage-dependent $Ca^{2+}$ channels, nonselective $Ca^{2+}$-permeable channels, and the reversed mode of operation of the $Na^{+}/Ca^{2+}$ exchanger. Recent studies have also demonstrated that some non-NMDA channels, such as the AMPA type, can have a relatively high $Ca^{2+}$ permeability in defined types of hippocampal neurons (Koh et al., 1995). Therefore, activation of these $Ca^{2+}$ conductances could cause more substantial extracellular $Ca^{2+}$ depletion in the cleft than predicted by our current model, and their contributions deserve to be evaluated in further refinements of the model.

The simulations assessing the contribution of different factors revealed that the extent of extracellular $Ca^{2+}$ depletion in the cleft can vary substantially as a function not only of stimulation frequency but also of membrane voltage, spine size, etc. Synaptic membrane depolarization and structural changes in spine morphology are important for generation of LTP and other forms of synaptic plasticity (Bliss and Collingridge, 1993), and therefore their relationships along with the changes in extracellular $Ca^{2+}$ dynamics in the cleft during high frequencies of stimulation may play a role in feedback regulation of synaptic activity.

Because trains of 10–100 pulses at 100 Hz are usually applied to induce LTP (Bliss and Collingridge, 1993) in the type of synapse modeled here, it is possible that these frequency-dependent changes in extracellular $Ca^{2+}$ within the synaptic cleft may bear some relationship to the mechanism of LTP generation. The decrease in extracellular $Ca^{2+}$ in the cleft will coincide with $Ca^{2+}$ influx through the activated GRC into the postsynaptic compartment of the spine and, therefore, may serve as a retrograde signal if there is a extracellular $Ca^{2+}$ sensor on the presynaptic membrane.

Such a mechanism, if it is related to the frequency-dependent changes in extracellular $Ca^{2+}$ within the synaptic cleft that are predicted by our model, may have important

functional implications. Because so many processes involved in synaptic transmission are dependent upon defined levels of extracellular $Ca^{2+}$, one might expect that a transitory decrease in extracellular $Ca^{2+}$ at high stimulation frequencies, by reducing the electrochemical gradients across both membranes, would have a nonspecific negative impact on synaptic transmission. There is, in contrast, usually synaptic facilitation under these conditions. In the discussion that follows, we propose that extracellular $Ca^{2+}$ serves a specific messenger function, because of the presence of CaRs within or in close proximity to the synaptic cleft, where they sense specific signals encoded by frequency-dependent changes in extracellular $Ca^{2+}$.

The parathyroid cell shows a steep inverse relationship between extracellular $Ca^{2+}$ and the secretion of parathyroid hormone (PTH) (Brown, 1991). Activation of the CaR due to an elevation in extracellular $Ca^{2+}$ leads to inhibition of PTH release, whereas the latter is stimulated by a reduction in extracellular $Ca^{2+}$ (Brown, 1991; Brown et al., 1993). Within the brain the CaR is located in nerve terminals and dendrites of the hippocampus (Ruat et al., 1995) and could potentially modulate synaptic processes by sensing activity-dependent changes in extracellular $Ca^{2+}$ within the synaptic cleft (Ruat et al., 1995; Brown et al., 1995). If, as in the parathyroid, presynaptic CaRs inhibit the secretion of neurotransmitter(s), a reduction in extracellular $Ca^{2+}$ in the synaptic cleft would be expected to stimulate neuromediator release. In this manner, through actions mediated by the CaR, extracellular $Ca^{2+}$ could function as a retrograde messenger. By sensing very small changes in extracellular $Ca^{2+}$ within the cleft due to $Ca^{2+}$ influx into the spine through NMDA and other $Ca^{2+}$-permeable channels, the CaR could further enhance synaptic transmission by "disinhibiting" the release of glutamate or other neuromediators. Such a messenger system would provide information directly to presynaptic terminals concerning the amount of $Ca^{2+}$ entering the postsynaptic compartment. In this formulation, the more pronounced reductions in extracellular $Ca^{2+}$ within the cleft predicted by our model at high frequencies would be associated with a more marked potentiation of glutamate release.

Because of the coupling of the CaR to G proteins, several second messenger pathways could mediate the inhibition of neurotransmitter secretion postulated above. For example, we have previously shown that activation of the CaR in parathyroid cells produces large increases in the levels of $IP_4$ (Hawkins et al., 1989), and Llinas and co-workers have recently found that microinjection of IP into the giant squid axon inhibits neurotransmitter release (Llinas et al., 1994). Therefore, the reductions in extracellular $Ca^{2+}$ within the synaptic cleft predicted by our model at high frequencies of stimulation might produce a CaR-mediated stimulation of neurotransmitter release via the associated reduction in $IP_4$ in the presynaptic terminals. In addition, $PIP_2$ has recently been suggested to play a key role in "priming" the exocytotic process (Hay et al., 1995). Therefore, the CaR-mediated reduction in $PIP_2$ under basal conditions might also serve to tonically inhibit neurotransmitter release. Exocytosis of neurotransmitters can also be modulated by cAMP (Bliss and Collingridge, 1993), which could likewise be involved in CaR-mediated regulation of synaptic function, because the CaR is coupled to inhibition of adenylate cyclase (Brown, 1991). Therefore, like mGluRs 2 and 3 (Yoshino and Kamiya, 1995), the CaR might inhibit neurotransmitter release at basal levels of extracellular $Ca^{2+}$, possibly by tonic, CaR-mediated inhibition of cAMP levels, with a reduction in this effect when extracellular $Ca^{2+}$ in the synaptic cleft decreased at high frequencies of stimulation.

The remarkable sensitivity of the CaR to small changes in extracellular $Ca^{2+}$ is a by-product of the steep sigmoidal relationship between its activity and the level of extracellular $Ca^{2+}$ (Brown, 1991; Brown et al., 1993, 1995). The midpoint for CaR activation is in the range of 1.25–1.3 mM extracellular $Ca^{2+}$ for the parathyroid cell in vivo, but in other tissues and especially in isolated cells it might be shifted to the right to varying extents, particularly when defined in terms of CaR-induced alterations in the levels of second messengers. Although this characteristic is not well known for the brain CaR, it is possible to assume a value of 1.45 mM. The CaR will tend to be in an activated state above this value, but at lower values it will be less active. With its steep sigmoid dependence on extracellular $Ca^{2+}$ it may act as a switch for the modulation of synaptic activity as a function of $Ca^{2+}$ availability in the cleft. To consider the contribution of this characteristic of the CaR to different modes of synaptic plasticity, horizontal lines were drawn at the level of 1.45 mM $Ca^{2+}$ for the simulations at different frequencies in Fig. 2. It appears that at frequencies higher than 10 Hz the CaR will be predominantly in an inactive state (Figs. 2 *D-F*), which, because of the putative inverse relationship to neurotransmitter release, may be associated with generation of LTP. At 10 Hz the CaR will spend equal amounts of time in the inactive and activated states (Fig. 2 *C*), and therefore no apparent change in synaptic plasticity will occur, which is consistent with the finding that stimulation at this frequency does not induce long-term modifications in synaptic transmission in studies on homosynaptic plasticity (Dudek and Baer, 1992). At lower frequencies, especially at 3 Hz (Fig. 2 *A*), the CaR is exposed most of the time to levels of extracellular $Ca^{2+}$ higher than the midpoint level of 1.45 mM, and therefore it will reside predominantly in an activated state. This may be associated with induction of long-term depression (LTD), which is consistent with the finding that stimulation at 3 Hz causes LTD in the same synapses in the CA1 area of hippocampus, in which tetanization at 100 Hz for 1 s generates LTP (Dudek and Baer, 1992). In simulations including higher values for the rates of $Ca^{2+}$ pump and $Na^+/Ca^{2+}$ exchange, after the initial extracellular $Ca^{2+}$ reduction after each stimulation at 3 Hz, extracellular $Ca^{2+}$ returned in 200–300 ms to levels substantially above the basal one (data not shown), which may generate more pronounced LTD. These elevated levels of extracellular $Ca^{2+}$ at low frequency stimulations may cor-

respond to the experimentally observed overshoots of extracellular $Ca^{2+}$ from 1.6 to 2.2 mM in hippocampal slices, which have been attributed to the activation of these $Ca^{2+}$ efflux systems by the increased $Ca^{2+}$ influx through GRC after the stimulation (Arens et al., 1992). In this way, the CaR may be involved in the induction of both forms of synaptic plasticity, LTP and LTD.

In summary, we have employed computer modeling to assess the impact of activation of $Ca^{2+}$-permeable channels in the postsynaptic membrane on the level of extracellular $Ca^{2+}$ within the synaptic cleft. The simulations indicate that substantial depletions of extracellular $Ca^{2+}$ in the cleft can occur during high frequencies of stimulation, whereas only minimal changes in extracellular $Ca^{2+}$ are observed at low frequencies. These frequency-dependent alterations in extracellular $Ca^{2+}$ dynamics may play a role in the modulation of different forms of synaptic plasticity, and thus the extracellular $Ca^{2+}$-sensing receptor could potentially serve as a key component of a simple mechanism of direct frequency detection and retrograde signaling.

We thank S. Y. Birzon and P. P. Vassilev for their excellent technical assistance, as well as their contribution to computer simulations and help in preparation of the manuscript.

This work was supported by generous grants from the U.S. Public Health Service (DK41415 to EMB and PMV and DK44588 and DK48330 to EMB), NPS Pharmaceuticals (to EMB), the St. Giles Foundation (to EMB and PMV); a National Science Foundation graduate fellowship (to JM); and Theodore and Vada Stanley Foundation and NARSAD (to PMV).

## REFERENCES

Almers, W., R. Fink, and P. T. Palade. 1981. Calcium depletion in frog muscle tubules: the decline of calcium current under maintained depolarization. *J. Physiol. (Lond.).* 312:177–207.

Arens, J., J. Stabel, U. Heinemann. 1992. Pharmacological properties of excitatory amino acid induced changes in extracellular calcium concentration in rat hippocampal slices. *Can. J. Physiol. Pharmacol.* 70: S194–S205.

Ascher, P., P. Bregestovski, and L. Nowak. 1988. *N*-Methyl-D-aspartate-activated channels of mouse central neurons in magnesium-free solutions. *J. Physiol. (Lond.).* 399:207–226.

Bekkers, J. M., and C. F. Stevens. 1989. NMDA and non-NMDA receptors are co-localized at individual excitatory synapses in cultured rat hippocampus. *Nature.* 341:230–233.

Bekkers, J. M., and C. F. Stevens. 1990. Presynaptic mechanism for long-term potentiation in the hippocampus. *Nature.* 346:724–729.

Bers, D. M. 1983. Early transient depletion of extracellular Ca during individual cardiac muscle contractions. *Am. J. Physiol.* 244:H462–H468.

Bers, D. M., and A. Peskoff. 1991. Diffusion around a cardiac calcium channel and the role of surface bound calcium. *Biophys. J.* 59:703–721.

Bliss, T. V. P., and G. L. Collingridge. 1993. A synaptic model of memory: long-term potentiation in the hippocampus. *Nature.* 361:31–39.

Bolshakov, V., and S. A. Siegelbaum. 1994. Postsynaptic induction and presynaptic expression of hippocampal long-term depression. *Science.* 264:1148–1152.

Brown, E. M. 1991. Extracellular $Ca2^{+}$ sensing, regulation of parathyroid cell function, and role of $Ca2^{+}$ and other ions as extgracellular (first) messengers. *Physiol. Rev.* 71:371–411.

Brown, E. M., G. Gamba, D. Riccardi, M. Lombardi, R. Butters, O. Kifor, A. Sun, M. A. Hediger, J. Lytton, and S. C. Hebert. 1993. Cloning and characterization of an extracellular $Ca^{2+}$-sensing receptor from bovine parathyroid. *Nature.* 71:575–580.

Brown, E. M., P. M. Vassilev, and S. C. Hebert. 1995. Calcium ions as extracellular messengers. *Cell.* 83:679–682.

Carafoli, E. 1987. Intracellular calcium homeostasis. *Annu. Rev. Biochem.* 56:395–433.

Cleeman, L., G. Pizarro, and M. Morad. 1984. Optical measurements of extracellular calcium depletion during a single heartbeat. *Science.* 226: 174–177.

Clements, J. D. 1990. Transmitter timecourse in the synaptic cleft: its role in central synaptic function. *Trends Neurosci.* 19:163–171.

Crank, J. 1975. The Mathematics of Diffusion. Oxford University Press, New York.

Crank, J., and P. Nicolson. 1947. A practical method for numerical evaluation of solutions of partial differential equations of the heat conduction type. *Proc. Cambr. Philos. Soc.* 43:50–64.

Dresdner, K. P., and R. P. Kline. 1985. Extracellular calcium ion depletion in frog cardiac ventricular muscle. *Biophys. J.* 48:33–45.

Dudek, S. M., and M. F. Baer. 1992. Homosynaptic long-term depression in area CA1 of hippocampus and effects of *N*-methyl-D-aspartate receptor blockade. *Proc. Natl. Acad. Sci. USA.* 89:4363–4367.

Gamble, E., and C. Koch. 1987. The dynamics of free calcium in dendritic spines in response to repetitive synaptic input. *Science.* 236:1311–1315.

Hamon, B., and U. Heinemann. 1986. Effects of GABA and bicuculline on *N*-methyl-D-aspartate- and quisqualate-induced reductions in extracellular free calcium in area CA1 of the hippocampal slice. *Exp. Brain Res.* 64:27–36.

Harris, K. M., and J. K. Stevens. 1989. Dendritic spines of CA1 pyramidal cells in the rat hippocampus: serial electron microscopy with reference to their biophysical characteristics. *J. Neurosci.* 9:2982–2997.

Hawkins, D., P. Enyedi, and E. M. Brown. 1989. The effects of high extracellular $Ca^{2+}$ and $Mg^{2+}$ concentrations on the levels of inositol 1,3,4,5-tetrakisphosphate in bovine parathyroid cells. *Endocrinology.* 124:838–844.

Hay, J. C., P. L. Fisette, G. H. Jenkins, R. A. Anderson, and T. F. J. Martin. 1995. ATP-dependent inositide phosphorylation required for $Ca^{2+}$-activated secretion. *Nature.* 374:173–177.

Hilgemann, D. W. 1986. Extracellular calcium transients at single excitations in rabbit atrium measured with tetramethylmurexide. *J. Gen. Physiol.* 87:707–735.

Hodgkin, A. L., and R. D. Keynes. 1957. Movements of labelled calcium in squid giant axons. *J. Physiol. (Lond.).* 138:253–281.

Holmes, W. R. 1990. Is the function of dendritic spines to concentrate calcium? *Brain Res.* 519:338–342.

Holmes, W. R., and W. B. Levy. 1990. Insights into associative long-term potentiation from computational models of NMDA receptor-mediated calcium influx and intracellular calcium concentration changes. *J. Neurophysiol.* 63:1148–1168.

Jahr, C. E., and C. F. Stevens. 1993. Calcium permeability of the *N*-methyl-D-aspartate receptor channel in hippocampal neurons in culture. *Proc. Natl. Acad. Sci. USA.* 90:11573–11577.

Kargacin, G. J. 1994. Calcium signaling in restricted diffusion spaces. *Biophys. J.* 67:262–272.

Kargacin, G., and F. S. Fay. 1991. $Ca^{2+}$ movement in smooth muscle cells studied with one- and two-dimensional diffusion models. *Biophys. J.* 60:1088–1100.

Kitajima, T., and K. Hara. 1990. A model of the mechanisms of long-term potentiation in the hippocampus. *Biol. Cybern.* 64:33–39.

Koch, C., and A. Zador. 1993. The function of dendritic spines: devices subserving biochemical rather than electrical compartmentalization. *J. Neurosci.* 13:413–422.

Koh, D.-S., J. R. P. Geiger, P. Jonas, and B. Sakmann. 1995. $Ca^{2+}$-permeable AMPA and NMDA receptor channels in basket cells of rat hippocampal dentate gyrus. *J. Physiol. (Lond.).* 485.2:383–402.

Kushmerick, M. J., and R. J. Podolsky. 1969. Ionic mobility in muscle cells. *Science.* 166:1297–1298.

Llinas, R., M. Sugimori, E. J. Lang, M. Morita, M. Fukuda, M. Niinobe, and K. Mikoshiba. 1994. The inositol high-polyphosphate series blocks synaptic transmission by preventing vesicular fusion: a squid giant synapse study. *Proc. Natl. Acad. Sci. USA.* 91:12990–12993.

Lucke, A., R. Kohling, H. Straub, D. Moskopp, H. Wassmann, and E.-J. Speckmann. 1995. Changes of extracellular calcium concentration in-

duced by application of excitatory amino acids in the human neocortex in vitro. *Brain Res.* 261:222–226.

Malenka, R. C., J. A. Kauer, R. S. Zucker, and R. A. Nicoll. 1988. Postsynaptic calcium is sufficient for potentiation of hippocampal synaptic transmission. *Science.* 242:81–84.

Malgaroli, A., and R. W. Tsien. 1992. Glutamate-induced long-term potentiation of the frequency of miniature synaptic currents in cultured hippocampal neurons. *Nature.* 357:134–139.

Malinow, R., and R. W. Tsien. 1990. Presynaptic enhancement shown by whole-cell recordings of long-term potentiation in hippocampal slices. *Nature.* 346:177–180.

Mascagny, M. V. 1989. Numerical methods for neuronal modeling. *In* Methods in Neuronal Modeling. C. Koch and I. Segev, editors. MIT Press, Cambridge. 439–484.

Nasi, E., and D. Tillotson. 1985. The rate of diffusion of $Ca^{2+}$ and $Ba^{2+}$ in a nerve cell body. *Biophys. J.* 47:735–738.

Niedergerke, R. 1957. The rate of action of calcium ions on the contraction of the heart. *J. Physiol. (Lond.).* 138:506–515.

Qian, N., and T. J. Sejnowski. 1989. An electrodiffusion model for computing membrane potentials and ionic concentrations in branching dendrites, spines and axons. *Biol. Cybern.* 62:1–15.

Riccardi, D., J. Park, W.-S. Lee, G. Gamba, E. M. Brown, and S. Hebert. 1995. Cloning and functional expression of a rat kidney extracellular calcium-sensing receptor. *Proc. Natl. Acad. Sci. USA.* 92:131–135.

Rogers, M., and J. A. Dani. 1995. Comparison of quantitative calcium flux through NMDA, ATP, and Ach receptor channels. *Biophys. J.* 68: 501–506.

Ruat, M., M. E. Molliver, A. M. Snowman, and S. H. Snyder. 1995. Calcium sensing receptor: molecular cloning in rat and localization to nerve terminals. *Proc. Natl. Acad. Sci. USA.* 92:3161–3165.

Schiegg, A., W. Gerstner, R. Ritz, and J. L. van Hemmen. 1995. Intracellular $Ca^{2+}$ stores can account for the time course of LTP induction: a model of $Ca^{2+}$ dynamics in dendritic spines. *J. Neurophysiol.* 74: 1046–1055.

Schneggenburger, R., Z. Zhou, A. Konnerth, and E. Neher. 1993. Functional contribution of calcium to the cation current through glutamate receptor channels. *Neuron.* 11:133–143.

Shepherd, G. 1996. The dendritic spine: a mutifunctional integrative unit. *J. Neurophysiol.* 75:2197–2210.

Spruston, N., P. Jonas, and B. Sakmann. 1995. Dendritic glutamate receptor channels in rat hippocampal CA3 and CA1 pyramidal neurons. *J. Physiol. (Lond.).* 482.2:325–352.

Sudhof, T. C. 1995. The synaptic vesicle cycle: a cascade of protein-protein interactions. *Nature.* 375:645–653.

Yoshino, M., and H. Kamiya. 1995. Suppression of presynaptic calcium influx by metabotropic glutamate receptor agonists in neonatal rat hippocampus. *Brain Res.* 695:179–185.

Zador, A., and C. Koch. 1994. Linearized models of calcium dynamics: formal equivalence to the cable equation. *J. Neurosci.* 14:4705–4715.

Zador, A., C. Koch, and T. H. Brown. 1990. Biophysical model of a Hebbian synapse. *Proc. Natl. Acad. Sci. USA.* 87:6718–6722.